Optical Fiber Technology 85 (2024) 103815

Contents lists available at ScienceDirect

Optical Fiber Technology

journal homepage: www.elsevier.com/locate/yofte

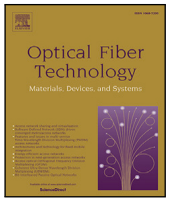

Regular Articles

Impact of the reconfigurable optical add-drop multiplexer architecture on the design of multi-band C+L+S optical networks

João Frederico Ó Ramos [a,*], Luís Cancela [a,b], João Rebola [a,b]

[a] Iscte - Instituto Universitário de Lisboa, Lisbon, Portugal
[b] Optical Communications and Photonics Group, Instituto de Telecomunicações, Lisbon, Portugal

ARTICLE INFO

Keywords:
Optical networks
Multi-band
Reconfigurable optical add-drop multiplexer
All-optical wavelength converter
Cost-per-bit
Physical layer impairments

ABSTRACT

The main advantage of multi-band (MB) networks is to provide more capacity than C-band networks by using other unused bands like the L- and S-bands and, in this way, postpone the announced optical network capacity crunch. However, MB nodes have a more complex structure than C-band nodes, impacting their cost and enhancing their induced physical layer impairments (PLIs). The main goal of this paper is to analyze the impact of several MB node architectures (namely baseline, common-band and compact MB node architectures) on the total network capacity and total network cost-per-bit, using a routing, modulation format, and spectrum assignment (RMSA) network planning tool based on a Monte–Carlo simulation that also incorporates the impact of network PLIs. When the PLIs are neglected, the common-band architecture presents the lowest cost-per-bit compared to the remaining MB architectures, since only lower cost C-band components are used. However, with the PLIs impact, the common-band architecture leads to the lowest total network capacity and highest cost-per-bit due to additional noise coming from all-optical wavelength converters. In particular, the common-band total network capacity is less than half the baseline and compact total network capacities for a blocking probability of 1%, considering the best channel launch power. Also, the common-band cost-per-bit is almost twice the baseline and compact cost-per-bit due to the PLIs-induced degradation.

1. Introduction

A capacity crunch has already been predicted several years ago regarding optical networks operating on the C-band, despite the huge technological advances and efforts that have been made to use the C-band with greater efficiency, e.g. coherent detection, flexible grid, symbol rate and modulation format adaptation [1]. The main drivers towards this critical scenario have been the emergence of new services, such as autonomous driving, virtual reality, cloud services, datacenter communications, and 5G services. Two solutions have been being investigated and tested over these last years for overcoming this capacity crunch: the multi-band (MB) solution that consists in the exploitation of the full low attenuation spectrum available in a single optical fiber, allowing transmission beyond the C-band, and is seen as a near to medium-term solution to solve the capacity problem [2,3]; and the spatial division multiplexing (SDM) solution, seen as a more long-term solution, that explores the spatial dimension to increase capacity, e.g. through multi-core, multi-mode, or multi-parallel fibers [4,5]. Optical network coding has been also proposed to overcome the capacity crunch due to its higher spectral efficiency and improved saving of network resources [6]. However, optical network coding relies on a different paradigm than nowadays optical networks, where individual wavelengths are simply routed end-to-end. For optical network coding, the intermediate nodes must have optical signal processing capabilities. Since most optical signal processing techniques are bulky and serious challenges must be surpassed for their photonic integration, [7], the practical realization of optical network coding seems far less immediate than SDM or the MB solution.

The MB solution, despite ultimately providing less capacity than the SDM solution, has a decisive cost advantage since it can reuse the vast already installed fiber. So, in the last couple of years, several MB transmission experiments and MB network scenarios have been tested and some C+L band transmission scenarios are already being used in commercial systems [8]. However, MB networks raise novel questions and concerns compared to C-band networks [2], like the equipment used on other bands not being so mature and with characteristics not yet optimized, the different fiber attenuations for each band, the performance degradation induced by the inter-channel stimulated Raman scattering (ISRS) on signal transmission and the proper design of the MB reconfigurable optical add-drop multiplexer (ROADM) node

* Corresponding author.
E-mail address: Frederico_O@iscte-iul.pt (J.F.Ó Ramos).

https://doi.org/10.1016/j.yofte.2024.103815
Received 12 January 2024; Received in revised form 15 March 2024; Accepted 24 April 2024

architecture, both in terms of cost and physical layer impairments (PLIs).

Several studies have already addressed the performance of MB networks considering the impact of the nodes architectures, e.g. [9–12]. In [11], a C+L+S network scenario based on the NSFNET topology is studied and a cost analysis is performed considering both transmission and node architecture issues. The node architectures considered were the MB baseline, which is the most common MB node where switching between bands is not allowed and the MB common-band architecture, which uses mainly C-band components [9]. In [10], a MB network scenario, based again on a NSFNET topology with MB all-optical wavelength converter (AO-WC) nodes and MB common-band nodes, is considered and a network planning tool that can adapt the transmission bands link-by-link is developed. In [12], a MB network experimental set-up is built with two MB nodes with an architecture called compact architecture that only uses components that work simultaneously in all bands and a network performance analysis has been carried out. From all the works just mentioned, it can be observed that, at least, four different MB nodes can be used in MB networks. Since the MB ROADM node is a key component in the overall network cost and network performance, it is essential to know what is the most cost-effective MB node, as well as the node less impacted by PLIs, which to the authors best knowledge has not been done yet.

So, the main purpose of this work is to develop a planning tool capable of solving the routing, modulation format, and spectrum assignment (RMSA) problem in a MB network, having in mind the PLIs and the ROADM node architecture. In our simulations, we consider two network topologies, the BT-UK [13] and CONUS-60 [14] networks, and three MB ROADM nodes – baseline, common-band and compact, considering the C+L+S bands and having in mind the most relevant PLIs – the insertion losses (ILs) of the components, the amplified spontaneous emission (ASE) noise of the optical amplifiers, the non-linear interference (NLI) noise, as well as the influence of the ISRS on signal transmission. The simulator output will provide a total network capacity and cost-per-bit assessment as a function of the ROADM node architecture for various network scenarios.

This paper is organized as follows. In Section 2, the four MB ROADM architectures are presented, and their internal structure is highlighted. The MB ROADM architectures cost-per-bit and ILs are also assessed and compared. In Section 3, the MB network planning tool is presented and the main assumptions, as well as the network metrics, are described. In Section 4, the total network capacity and total network cost-per-bit are discussed as a function of the MB ROADM architecture, considering the BT-UK and CONUS-60 networks. Section 5 presents the main conclusions.

2. C+L+S MB ROADMs

This section starts by studying and presenting the four ROADM architectures proposed for MB networks. These four MB ROADM architectures are, then, compared in terms of cost-per-bit, and the insertion losses are also computed for the MB ROADM architectures with the lower cost-per-bit.

2.1. ROADM internal structure

Four C+L+S MB architectures are studied in this subsection regarding their internal structure. The four C+L+S MB architectures, shown in Fig. 1, consider a *R*-degree (number of directions) route and select (R&S) architecture, and are the baseline architecture [9,11], AO-WC architecture [10], common-band architecture [9–11], and compact architecture [2,12].

Fig. 1a shows the MB baseline architecture, where each degree has a MB demultiplexer (MB-DEMUX) and MB multiplexer (MB-MUX), optical amplifiers (two Erbium-doped fiber amplifiers (EDFAs) for the C- and L-bands and one Thulium-doped fiber amplifier (TDFA) for the S-band), and an input bank of parallel dedicated-band wavelength selective switches (WSSs), which are connected to dedicated-band WSSs at the output ROADM directions [9,11]. In this architecture, the wavelengths can be switched to any direction within each band, but switching between bands is not possible. The ROADM management and maintenance may become complex due to the large amount of equipment needed for each band [2,11]. As an advantage, the equipment dedicated to other bands may not be acquired when network traffic is low, especially in the beginning of network operation [2].

To add the possibility of switching between bands, the MB AO-WC (Fig. 1b), MB common-band (Fig. 1c), and MB compact (Fig. 1d) architectures were proposed in several works, e.g. [2,9–12]. The MB AO-WC shown in Fig. 1b has an AO-WC after each route WSS, which converts multiple wavelengths from one band to another. In this architecture, as happens with the MB baseline architecture, equipment dedicated to other bands may not be acquired in the beginning of the network operation [2], and the use of dedicated components for each band is required. In addition, the number of AO-WCs per direction greatly increases when the node degree and the number of bands increase. The MB common-band architecture shown in Fig. 1c uses also AO-WCs. In this situation, the AO-WC is located before and after the C-band WSSs and has the function of converting multiple wavelengths to and from the C-band [9–11]. As switching inside the node is all performed in the C-band, this architecture uses only C-band components (in the express and A/D structures), decreasing the total node cost. Furthermore, the number of AO-WCs is lower than in the MB AO-WC architecture (as shown in the next subsection) [10], and the other bands equipment can be acquired in a phased way, depending on the network traffic evolution. The main disadvantage of the common-band and AO-WC architectures is the use of the AO-WCs, which are currently not in a commercial phase [11]. Finally, the MB compact architecture (Fig. 1d) uses, in the express structure, MB WSSs that work simultaneously in multiple bands to reduce the amount of equipment needed [2], and the MB OA is implemented with three OAs, one for each band. A disadvantage of this architecture is the high initial deployment investment, as the acquisition of MB components at the beginning of the network operation is required [2].

2.2. Cost analysis

The cost of each MB architecture is calculated in this subsection by assuming the components cost presented in Table 1. To compute the cost of each MB ROADMs, 64 channels are considered in each band (with a total of 192 channels in the 3 bands) with a 75 GHz channel spacing [15,16], and a colorless and directionless (CD) R&S ROADM architecture with an A/D ratio of 25% is assumed [17]. The components cost is normalized to the cost of the C-band EDFA, and is extracted from [11,13], with the parameters α and β defined as in [11]. The L-band components are assumed 20% more expensive than C-band components, and the cost of the S-band components depends on the multiplicative factor α, which indicates the cost increase concerning the C-band cost, ranging from 1.2 to 1.5. The AO-WC cost depends on the C-band transponder (TR) cost, with the parameter β ranging from 0.5 to 2 [11,13]. In the results presented, we considered the highest cost scenario, α=1.5 and β=2 [11].

The total cost of the CD A/D structure of the baseline, AO-WC, common-band and compact architectures is,

$$Cost_{A/D} = \sum_{b}^{N_{bands}} Cost_{A/D,b} \tag{1}$$

where $Cost_{A/D,b}$ is the cost of the A/D structure per band b (with b=C, L or S) of the MB ROADM given by [17],

$$\begin{aligned} Cost_{A/D,b} &= 2N_{A/D}Cost_{WSS,R\times 1,b} \\ &+2N_{A/D}Cost_{WSS,1\times M',b} + MCost_{TR,b} \end{aligned} \tag{2}$$

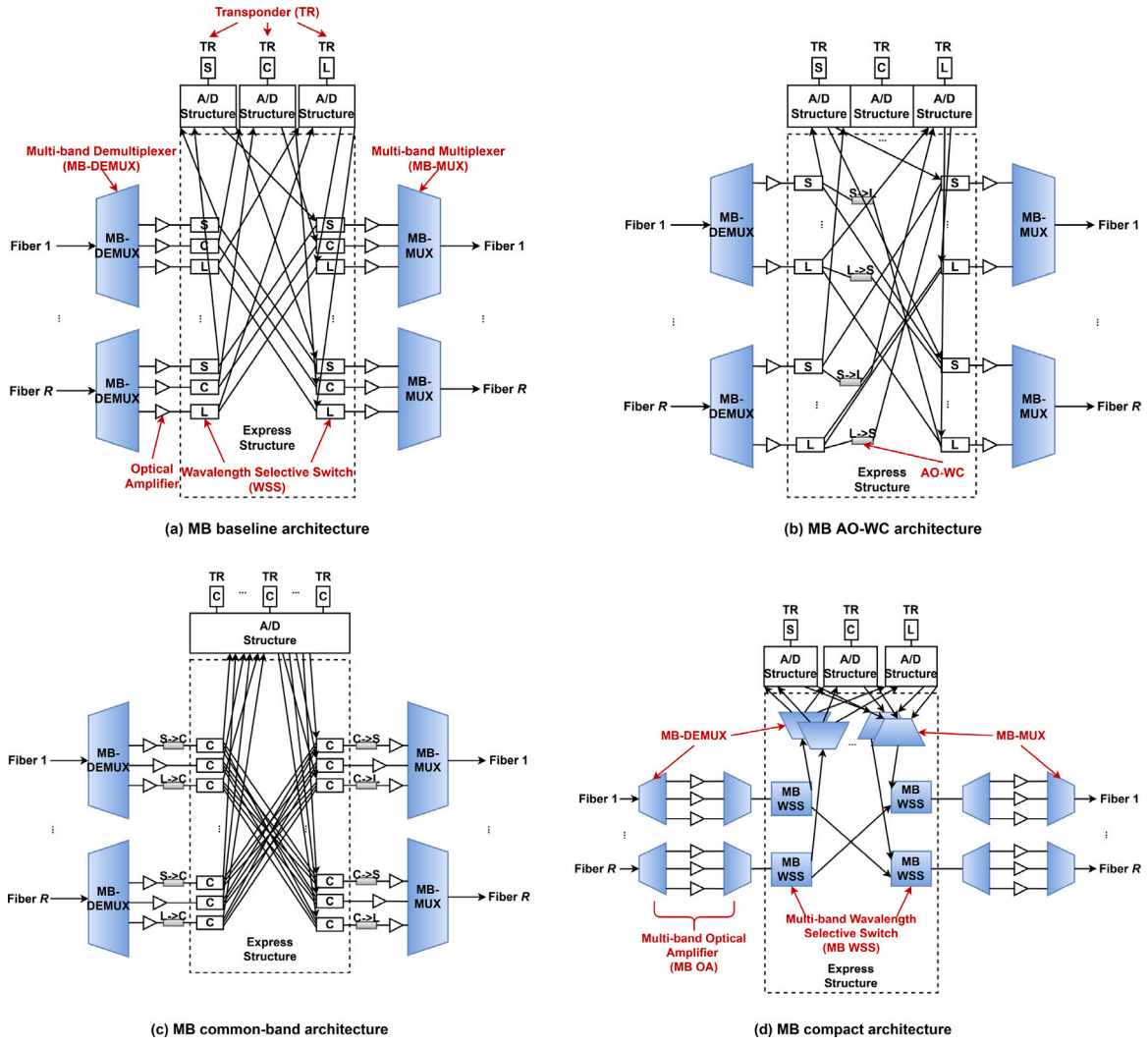

Fig. 1. *R*-degree MB R&S node architectures.

Table 1
Relative cost of components for C-, L- and S-bands.

Components	C-band	L-band	S-band	Variable name
EDFA	1	1.2	–	$Cost_{xDFA,b}$
TDFA	–	–	α	
1 × 2 WSS	1.25	1.5	1.25α	$Cost_{WSS,b}$
1 × 4 WSS	2.5	3	2.5α	
1 × 9 WSS	5	6	5α	
1 × 20 WSS	7.5	9	7.5α	
1 × 40 WSS	15	18	15α	
1 × 80 WSS	30	36	30α	
Transponder (TR)	36	43.2	36α	$Cost_{TR,b}$
MB Optical Amplifier		2.28+α		$Cost_{MB,OA}$
1×N_{bands} MB MUX/DEMUX		0.04		$Cost_{MB,MUX/DEMUX}$
AO-WC		36β		$Cost_{AO-WC}$
1 × 9 MB WSS		7α		$Cost_{MB,WSS}$
1 × 20 MB WSS		10α		
1 × 40 MB WSS		20α		

where $Cost_{WSS,R\times1,b}$, $Cost_{WSS,1\times M',b}$ and $Cost_{TR,b}$ is, respectively, the cost of the WSSs R×1, WSSs 1×M', and TRs as given in Table 1. Also, in Eq. (2), M is the total number of TRs and $N_{A/D}$ is the number of A/D cards, computed as the ratio between the total number of TRs (M) and the number of TRs per A/D card, which is determined by the number of WSS outputs of the A/D structure (M'). Note that for the baseline, AO-WC and compact architectures, the cost of A/D structure is computed for the C-, L- and S-bands (N_{bands}=3 and b=C, L and S), and in the case of the common-band architecture for the C-band only (N_{bands}=1 and b=C). The total cost of the express structure of the baseline, AO-WC and common-band architectures is given by [17],

$$Cost_{Express} = \sum_{b}^{N_{bands}} \{2R(Cost_{WSS,a} + Cost_{xDFA,b})\} + N_{AO-WC}Cost_{AO-WC} + 2RCost_{MB,MUX/DEMUX} \quad (3)$$

where $Cost_{WSS,a}$, $Cost_{xDFA,b}$, $Cost_{MB,MUX/DEMUX}$ and $Cost_{AO-WC}$ is, respectively, the cost of the WSSs, xDFAs (x=E or x=T), MUX/DEMUXs and AO-WCs as given in Table 1. Also, in Eq. (3), N_{AO-WC} is the number of AO-WCs and a=b, for the baseline and AO-WC architectures and a=C, for the common-band architecture. Note that for the baseline, AO-WC and common-band architectures, the total cost of the express structure is computed for the C-, L- and S-bands (N_{bands}=3). The express structure total cost of the MB compact architecture [17],

$$Cost_{Compact,Express} = 2R(Cost_{MB,WSS} + Cost_{MB,OA}) + 2RN_{A/D}Cost_{MB,MUX/DEMUX} \quad (4)$$

where $Cost_{MB,WSS}$, $Cost_{MB,MUX/DEMUX}$, and $Cost_{MB,OA}$ is, respectively, the cost of the MB WSSs, MUX/DEMUXs and OAs as given in Table 1.

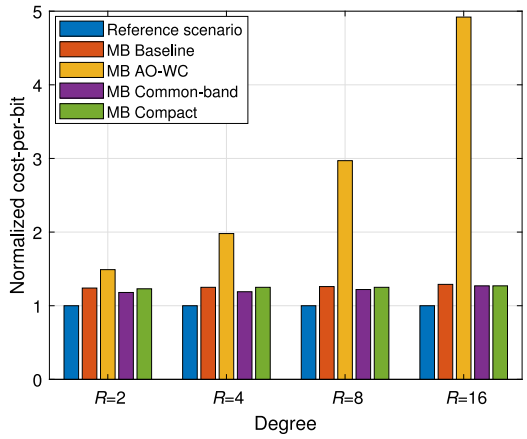

Fig. 2. Normalized cost-per-bit as a function of the ROADM degree for an A/D ratio of 25%, considering the four C+L+S MB architectures.

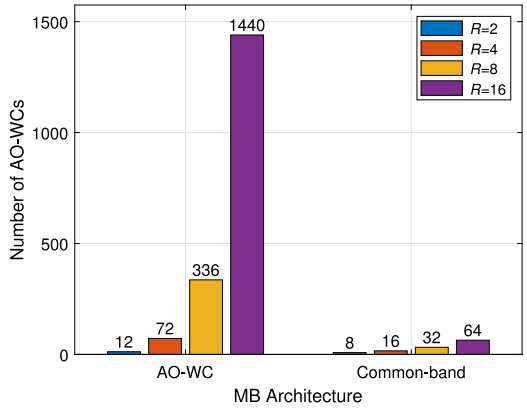

Fig. 3. Number of AO-WCs for AO-WC and common-band architectures considering the ROADM degrees, 2, 4, 8 and 16.

The total node cost ($Cost_{node}$) is computed by summing the total A/D structure cost given by Eq. (1) with the total express structure cost, given by Eq. (3), for the baseline, AO-WC and common-band architectures or by Eq. (4) for the compact architecture.

The cost-per-bit calculation for the four MB architectures is performed next and is defined as the ratio between the total node cost ($Cost_{node}$) and the total node A/D capacity, which depends on each TR bit rate (a bit rate of 100 Gbit/s per TR is assumed) and on the number of TRs (M). The normalized cost-per-bit as a function of the ROADM degree is shown in Fig. 2, for all the four studied MB architectures. The cost-per-bit is normalized to the cost of a reference scenario, which is a CD R&S C-band node with 2 directions, with a total node A/D capacity of 3.2 Tbit/s, for an A/D ratio of 25%.

From Fig. 2, it can be observed that the cost-per-bit of the MB baseline, common-band and compact architectures remain practically unchanged with the increase of the number of directions, since these architectures cost depends mainly on the TRs cost (the number of TRs roughly doubles with the number of directions — for R=2, 4, 8 and 16, the number of TRs is, respectively, 96, 192, 384 and 768). The MB common-band architecture presents a slightly lower cost-per-bit compared with the other two MB architectures, since it uses only C-band components in express and A/D structures. In the MB common-band architecture, the number of AO-WC doubles with the number of directions, as observed in Fig. 3, but their contribution to the total node cost is low. In the MB AO-WC architecture, the number of AO-WCs increases much more significantly with the number of directions as shown in Fig. 3, leading to a significant contribution to the total node cost when the number of directions increases. Hence, the MB AO-WC architecture is the most costly, and for this reason, it will not be considered in the analysis performed in the following sections. The results obtained in Fig. 2 for the MB baseline, and MB common-band, are very similar to the results of Figure 3 of [11], for α=1.5, β=2, when neglecting the fiber lease cost.

Table 2
Insertion losses of the baseline, common-band, and compact architectures for the C-, L- and S-bands, and LCoS WSSs.

Architecture	Insertion losses [dB]		
	C-band	L-band	S-band
Baseline	10	10	12
Common-band		10	
Compact	14	14	15

2.3. Insertion losses

The ILs introduced by the MB baseline, common-band, and compact architectures are assessed in this subsection. To accomplish this task, the different signal paths inside the ROADM architecture and the components that belong to those paths must be identified.

The optical components inside the MB architectures are the WSSs, AO-WCs, and MB-DEMUX/MUXs, as shown in Section 2.1. The typical ILs of each MB liquid crystal on silicon (LCoS) WSS for the C-, L- and S-bands are, respectively, 5 dB, 5 dB, and 6 dB, and the ILs of the C+L+S MB WSS are considered as 6 dB [18,19]. The AO-WCs considered in the common-band architecture are based on highly-nonlinear fibers (HNLF), which use four-wave mixing to achieve the wavelength conversion [10,20]. The HNLF-based AO-WC considered has a typical IL (the term conversion loss is used in [21]) of approximately 20 dB, which is compensated by an optical amplifier placed inside the AO-WC [20,22]. In the compact architecture, we also have in the A/D structure MB-DEMUX/MUXs, which we assume to have 3 dB of ILs [16].

In a ROADM, an optical signal can propagate through three possible optical paths — express, add, and drop paths. In particular, for the baseline and common-band architectures, the ILs of the express, add, and drop paths are the same because we are assuming that the ILs of the WSSs of the R&S stage are the same as the ILs of the $R\times M'$ WSS of the CD A/D structure [23]. So, the ILs of the baseline and common-band architectures do not depend on the optical path considered. However, in the compact architecture, the ILs of the express path are different from the ILs of the add and drop paths. In particular, in the express path, two MB WSSs, and in the add and drop paths, one MB WSS, MB-DEMUX/MUX, and a dedicated-band WSS, are used. In this situation, the ILs of the add and drop paths are higher than the ones of the express paths.

The ILs considered for the baseline, common-band, and compact architectures are shown in Table 2, and correspond to the highest ILs found along the possible optical paths within the node.

3. RMSA planning tool for C+L+S MB networks considering the impact of PLIs and node architecture

In this section, we present and explain the developed C+L+S MB network planning tool with the assumptions and the network metrics considered.

3.1. Planning tool flowchart

In this subsection, we present and discuss the flowchart of the C+L+S MB network simulator developed in Matlab, used to compute the total network capacity and total network cost-per-bit considering the PLIs and also the MB node architectures presented in Section 2. The

simulator solves the RMSA problem following the statistical network assessment process (SNAP) model for dynamic traffic considering a flexible grid C+L+S MB scenario [16,24]. SNAP uses a Monte Carlo (MC) simulation method, wherein in each MC iteration a high number of progressive random traffic demands is generated. Demands are then allocated according to the defined RMSA algorithm, and for each MC iteration, the blocking probability (BP), and the total network capacity can be computed [16,24].

The developed simulator, whose flowchart is presented in Fig. 4, has three main steps: offline computation of the available optical paths, routing and modulation format assignment and spectrum assignment. The simulator inputs are the network physical topology, channel launch power, target BP, MB node architecture, and the maximum number of randomly generated demands in each MC iteration, whereas the simulator outputs are, for example, the total network capacity and total network cost-per-bit.

In the first step of the simulator, offline computation of the available optical paths, the k-th shortest candidate paths for each possible demand and band are computed with the Yen's k-shortest path algorithm [25] using the metric based on the path length in km. For each one of the candidate paths, the ASE and NLI noise powers are computed for each band and modulation format. The total optical signal-to-noise ratio (OSNR) is calculated for all candidate paths, from the highest modulation format to the lowest, and it is checked if the computed residual margin is above a minimum residual margin [16,26] (further details in Section 3.2). If the target residual margin is met for a specific modulation format, the residual margin is not computed for the lower modulation formats, for that candidate path. However, if it is not possible to assign a modulation format to the candidate path (residual margin not met), that candidate path is discarded. Furthermore, if no candidate paths of a specific demand satisfy the residual margin, that path is not used, which means that optical regeneration should be used for this path [16]. After performing the modulation format assignment for all k-candidate paths, the k-candidate paths of each demand are sorted based on the OSNR in descending order.

In the next step, the routing and modulation format assignment, a demand is randomly chosen from the list of the available paths computed in the previous step, assuming a uniform distribution. For each randomly chosen demand, the candidate path with the highest modulation format is selected, which means that, in our simulator, the highest possible capacity is always used for each demand.

In the spectrum assignment step, the frequency slots (FSs) are assigned using the First-Fit (FF) algorithm. The FF algorithm starts looking for available FSs from the lower frequency channels of the C-band towards the L- and S-bands, and tries to assign contiguous FSs in every link along the optical path [10]. Note that for each band, if the FSs cannot be assigned for a particular candidate path, then the next candidate path must be chosen within each band. If there are no available FSs in any of the bands and any of the candidate paths, that demand is blocked, and the network BP is computed. If the BP is below the target BP, the FF algorithm tries to allocate FSs for the next randomly generated demand. If the computed BP is above the target, the total network capacity and cost-per-bit are computed and the simulator ends the present MC iteration and enters in the next MC iteration (not shown in Fig. 4). A maximum number of demands randomly generated, $N_{gen,max}$, is set for each MC iteration. The simulation ends when a specific number of MC iterations (N_{sim}) is reached.

3.2. Network physical layer model

In this subsection, the network physical layer model used in the planning tool presented in the previous subsection is described and the model assumptions are discussed. First, we have considered that the MB network transports 64 Gbaud signals, regardless of the modulation format, using a 75 GHz channel spacing [15,16]. So, in each band, 64 channels can be transported, corresponding to a total of 384 FSs, each one with 12.5 GHz (note that a 75 GHz channel spacing occupies 6 FSs). Also, there are two different bandgaps, the first one between the L- and C-bands, and the second one between the C- and S-bands, as shown in Fig. 5.

The performance of an optical channel m is assessed using the residual margin, computed in dB, with [26,27],

$$RM_p = OSNR_{m,p,b} - ROSNR - SM_p \tag{5}$$

where $OSNR_{m,p,b}$ is the OSNR measured at the end of a candidate path for channel m, candidate path p and band b, $ROSNR$ is the minimum required OSNR (ROSNR) and SM_p is the safety margin. The minimum residual margin is set to 2 dB [15]. The safety margin takes into account additional OSNR degradations resulting from aging, optical filtering, crosstalk, and other performance degrading effects, is computed in dB and given by [26,27],

$$SM_p = 0.05 \times (N_{OLAs} + N_{ROADMs}) + P_{filt} + P_{xtalk} \tag{6}$$

where N_{OLAs} and N_{ROADMs} are, respectively, the number of optical amplifiers and the number of ROADMs in candidate path p. This safety margin also considers the optical filtering penalty (P_{filt}) and the crosstalk penalty (P_{xtalk}). In this work, a worst-case crosstalk penalty of 0.5 dB is considered [27]. The optical filtering penalty depends on the number of WSSs (two times the number of ROADMs, since a R&S architecture is assumed for all the ROADM nodes) traversed by the optical signal in candidate path p and is extrapolated from the results presented in [28].

The OSNR at the end of a path for channel m, candidate path p and band b is calculated considering the ASE noise and the NLI noise powers, and is given in linear units by [15,16],

$$osnr_{m,p,b} = \frac{p_m}{\sum_{i=1}^{N_{i,p}} (p_{ASE,m,i,b} + p_{NLI,m,i,b})} \tag{7}$$

where $N_{i,p}$ is the number of links within the candidate path p, $p_{ASE,m,i,b}$ is the ASE noise power in channel m, $p_{NLI,m,i,b}$ is the NLI noise power in channel m, and p_m is the launch power of channel m. The NLI noise power is calculated using a closed-form approximation of the ISRS-Gaussian noise model that includes the modulation format correction [29–31], where the self-phase modulation and cross-phase modulation contributions are given, respectively, by Eqs. (10) and (11) of [29]. The ASE noise power is modeled as in [15,16]. The following assumptions are made: (1) incoherent accumulation of NLI noise along multiple fiber spans; (2) exact loss channel compensation m along the candidate path p; (3) PLIs are computed for the central channel in each band; (4) optical signal enters and leaves the node in the same band, i.e., no switching between bands inside the node is considered, which means that the accumulated ASE noise power is the same for all paths (note that this is true for the baseline architecture, but not true for the common-band and compact architectures, as different paths can have different ASE noise powers); (5) additional ASE noise from the optical amplifier located inside the AO-WC is taken into account in Eq. (7).

3.3. Network metrics

This subsection presents and explains the network metrics used, in particular the BP, the total network capacity, and the total network cost-per-bit.

The BP is computed by averaging the BPs obtained for all the N_{sim} MC iterations, and is given by [16],

$$BP = \frac{1}{N_{sim}} \sum_{i=1}^{N_{sim}} \frac{N_{blocked,demands,i}}{N_{total,demands,i}} \tag{8}$$

where $N_{blocked,demands,i}$ and $N_{total,demands,i}$ correspond, respectively, to the number of blocked demands and the total number of demands generated in the ith iteration of the MC simulator.

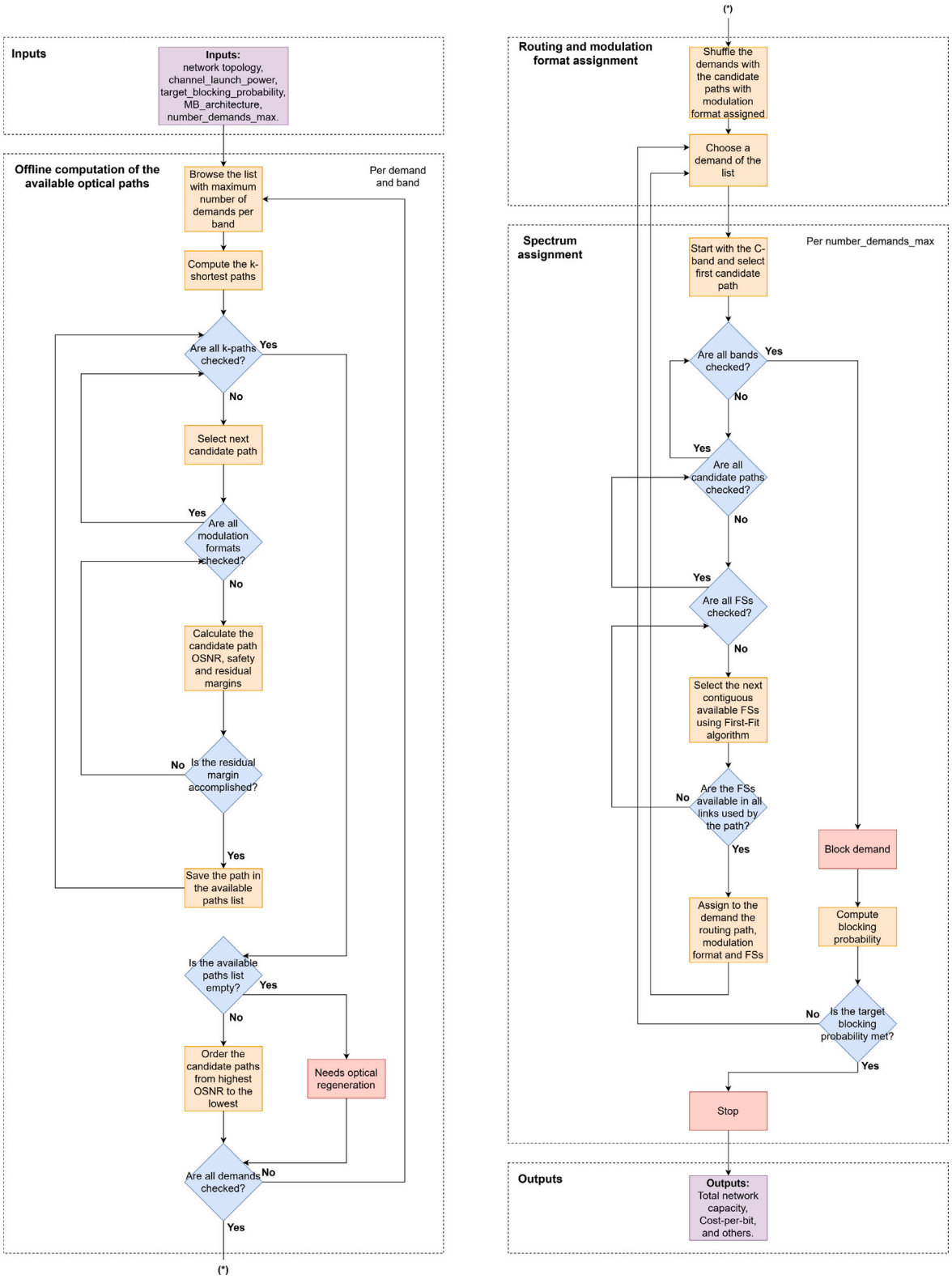

Fig. 4. Flowchart of the Matlab simulator used to solve the RMSA problem in a flexible grid C+L+S MB network aware of the PLIs and node architecture.

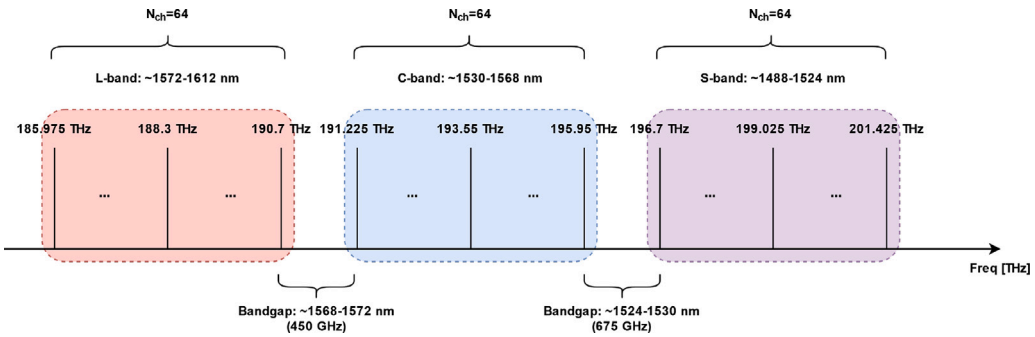

Fig. 5. Wavelength division multiplexing signal spectrum considered in the C-, L- and S-bands and corresponding ITU-T grid frequencies for a channel spacing of 75 GHz.

The total network capacity is given by [16],

$$Net_{capacity} = \frac{1}{N_{sim}} \sum_{i=1}^{N_{sim}} Net_{capacity,i} \tag{9}$$

where $Net_{capacity,i}$ is the total network capacity obtained in the i-th iteration of the MC simulator.

The total network cost-per-bit is computed with [11,13],

$$Cost_{perbit} = \frac{Net_{capacity}}{Cost_{Network,n}} \tag{10}$$

where $Cost_{Network,n}$ corresponds to the total cost of the network given by,

$$Cost_{Network,n} = \sum_{k=1}^{N_{Nodes}} Cost_{node,k} + 2Cost_{fiber}Total_{Length} \tag{11}$$

where n corresponds to the network topology, N_{Nodes} corresponds to the number of nodes of the network, $Cost_{fiber}$ corresponds to the fiber lease cost per km during 5 years [13] and $Total_{Length}$ corresponds to the total length of the fiber in the network in km. Note that in Eq. (11), the real degree of each node in each network topology has been considered.

4. Impact of the ROADM architecture on the total network capacity and cost-per-bit

This section presents the parameters considered to obtain the RMSA results using the simulator described in Section 3, for a C+L+S MB optical network scenario. It also presents and discusses the impact of the ROADM architecture on the total network capacity and total network cost-per-bit.

4.1. Network topologies and system parameters

In this work, we consider the BT-UK network, depicted in Fig. 6 [13] and the CONUS-60 network, depicted in Fig. 7 [14]. As shown in Table 3, the two network topologies have quite distinct physical and logical features. From this table, it is possible to see that the CONUS-60 topology allows a higher maximum number of logical paths (this number is computed assuming that there is a logical path between each node) compared to the BT-UK network, due to the larger network size (higher number of nodes and longer average link length). The BT-UK network is a smaller size network (lower number of network nodes and link length), but it has a higher average node degree indicating that it is more meshed.

In Table 4, the parameters used to perform the RMSA analysis of the BT-UK and CONUS-60 networks and the estimation of the total network capacity and total network cost-per-bit are presented. A standard optical fiber is considered and the pre- and in-line amplifier gains are set to compensate the link optical losses, assuming a maximum gain of 30 dB. The post-amplifier gain is set to compensate the ILs for each node architecture, shown in Table 2. Different amplifier noise figures are considered for each band. Table 5 presents the minimum required

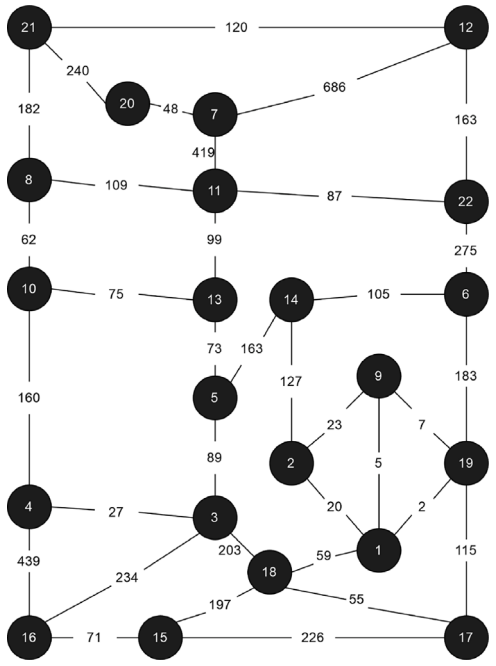

Fig. 6. Physical topology of the BT-UK network [13].

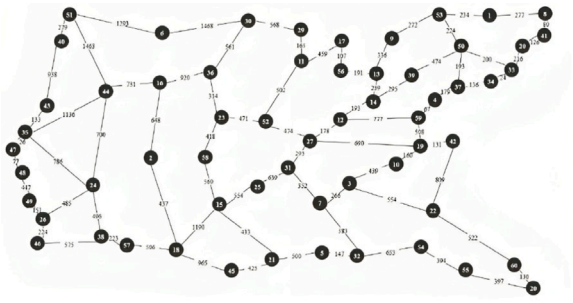

Fig. 7. Physical topology of the CONUS-60 network [14].

OSNR for the three modulation formats considered, quadrature-phase shift keying (QPSK), 8-quadrature amplitude modulation (QAM) and 16-QAM, and the corresponding bit rates considering a symbol rate of 64 Gbaud [16,32].

4.2. Physical layer impairments impact on the number of available paths

In this subsection, the impact of the PLIs on the number of available paths in the BT-UK and CONUS-60 networks is assessed. The number

Table 3
Physical and logical features of the network topologies BT-UK and CONUS-60.

Parameters	Network	
	BT-UK	CONUS-60
Maximum no. of logical paths	231	1770
Number of nodes	22	60
Number of links	35	79
Average node degree	3.2	2.6
Average link length [km]	147	445
Shortest link [km]	2	24
Longest link [km]	686	1468
Total network length [km]	5148	35 388

Table 4
System parameters considered for the RMSA tool.

Parameters	Values		
	C-band	L-band	S-band
Number of candidate paths		5	
Number of MC simulations (N_{sim})		50	
Max. number of demands randomly generated ($N_{gen,max}$)		5000	
BER (pre-FEC)		2×10^{-2}	
Channel spacing [GHz]		75	
Roll-off factor		0	
Total number of channels		192	
Number of channels per band		64	
Channel FSs spacing [GHz]		12.5	
Fiber attenuation) [dB/km]	0.185	0.185	0.2
Target residual margin [dB]		2	
Maximum amplifier gain [dB]		30	
AO-WC gain [dB]		20	
Post-amplifier gain of baseline node [dB]	10	10	12
Post-amplifier gain of common-band node [dB]		10	
Post-amplifier gain of compact node [dB]	14	14	15
Amplifier noise figure [dB]	4.25	4.68	6.40
Dispersion [ps/nm/km]		17	
Dispersion slope [fs/nm^2/km]		67	
Reference wavelength [nm]		1550	
Raman gain slope [1/W/km/THz]		0.028	
Nonlinear coefficient [1/W/km]		1.30	

Table 5
Minimum required OSNR and transport capacity of each modulation format.

Parameters	16-QAM	8-QAM	QPSK
ROSNR [dB]	16.9	13.9	8.9
Capacity [Gbit/s]	400	300	200

of available paths is computed for each band and MB architecture as a function of the channel launch power, and it is represented in Figs. 8 and 9, respectively, for the BT-UK and CONUS-60 networks. The number of available paths is obtained in the first step of the simulator and corresponds to the number of paths that meet the minimum residual margin.

It can be observed from Figs. 8 and 9, that the number of available paths that can be assigned for the baseline and compact architectures is very similar due to the high ASE noise introduced by the optical pre-amplifiers along the candidate path, which is similar for both architectures. Furthermore, the number of available paths in the C-band is equal for the baseline and common-band architectures, since both nodes have equal ILs in this band. In the common-band architecture, for the L- and S-bands, the number of available paths is generally much lower when compared to the other node architectures due to additional noise coming from the AO-WCs. Moreover, it can be observed that the optimum channel launch powers that lead to a higher number of available paths are roughly between 3 and 4 dBm for the C-band, between 2 and 3 dBm, for the L-band and between 5 and 6 dBm for the S-band, for both networks studied. The maximum number of available paths for the BT-UK network is 225, 216 and 212 and, for the CONUS-60 network, 375, 314 and 247, respectively, in the C-, L- and S-bands, considering the baseline architecture.

Comparing the maximum number of available paths obtained for both network topologies in Figs. 8 and 9 with the maximum number of logical paths given in Table 3, it is possible to see that with the BT-UK topology, the number of candidate paths is much closer to the maximum (231) than in the CONUS-60 network (1770) due to the lower average link length of the BT-UK topology, which allows that candidate paths meet the residual margin. In the CONUS-60 network, most of the optical paths require optical regeneration.

4.3. Total network capacity

This subsection presents the total network capacity estimated with Eq. (9) for the target BPs ranging from 1% to 10%. Figs. 10 and 11 show the total network capacity as a function of the BP for the baseline, common-band, and compact architectures considering, respectively the BT-UK and CONUS-60 network topologies for the channel launch powers of −2, 0 and 2 dBm.

From Figs. 10 and 11 similar conclusions can be drawn, regarding the different MB ROADM architectures: (1) the total network capacity is similar for the baseline and compact architectures due to the similar number of available paths, and (2) the total network capacity obtained for the common-band architecture is lower than the one obtained for the two other MB node architectures due to the lower number of available paths (see Figs. 8 and 9). In addition, specific conclusions can be drawn for each network topology. In the BT-UK network, for a BP above around 3%, the total network capacity obtained with the common-band architecture, as observed in Fig. 10, is at least 100 Tbit/s lower than the one obtained with the other two architectures. For the CONUS-60 network (Fig. 11), it can be seen that for a BP higher than 4% (common-band architecture) and 6% (baseline and compact architectures), the total network capacity for a 0 dBm channel launch power becomes lower than the capacities obtained for −2 dBm channel launch power. This behavior can be justified by noting that there are less available paths for a channel launch power of −2 dBm than for 0 dBm (Fig. 9), and as most of these paths share common links, due to the longer average link length of the CONUS-60 network. This leads to more congested links and, ultimately, more paths are blocked, and, the total transport capacity decreases for a higher channel launch power.

By comparing Figs. 10 and 11, the most notorious difference is the higher total network capacity obtained for the CONUS-60 network in comparison to the BT-UK, mainly due to the higher number of available paths (see Figs. 8 and 9). For a BP of 1%, the channel launch power that ensures the highest total network capacity for the baseline, common-band, and compact architectures is, respectively, −2 dBm (189 Tbit/s), 0 dBm (82 Tbit/s) and 0 dBm (173 Tbit/s). On the other hand, for the CONUS-60 network, the channel launch power of 0 dBm ensures the highest total network capacity for the baseline (275 Tbit/s), common-band (162 Tbit/s), and compact architectures (266 Tbit/s).

The results obtained in Figs. 10 and 11 can be compared with the results of Figure 7 (a) of [16], for the C+L+S 100 and 400 Gbit/s scenarios and the BPs of 1% and 10%. It can be observed that the total network capacities obtained in this work, for the baseline architecture (that corresponds to the MB architecture considered in [16]), and the CONUS-60 topology (similar to the US-NET topology, in terms of average link length [16]), are in the same order of magnitude as those obtained in [16]. For the 0 dBm channel launch power and the BP of

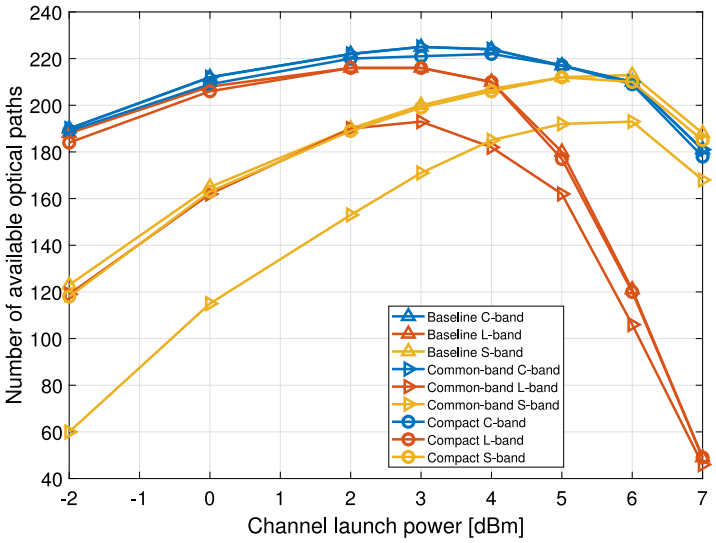

Fig. 8. Number of available paths as a function of the channel launch power, for the BT-UK network and for each MB node architecture.

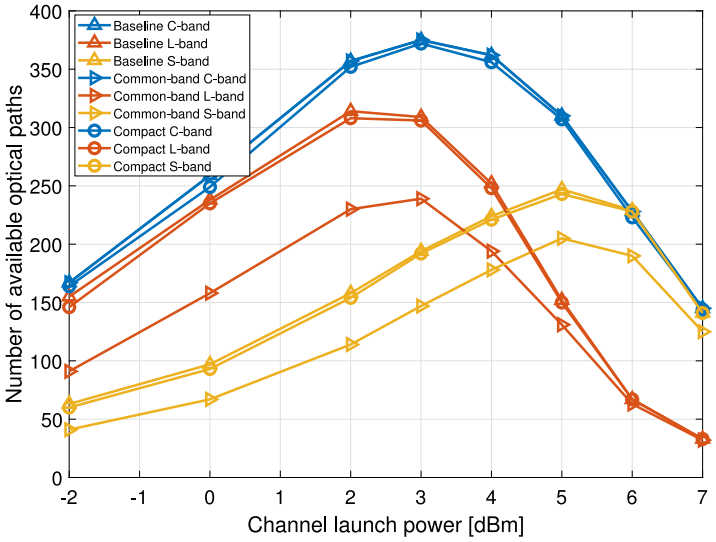

Fig. 9. Number of available paths as a function of the channel launch power, for the CONUS-60 network and for each MB node architecture.

1%, the total network capacity obtained in this work for the baseline architecture is 275 Tbit/s, compared with the total network capacity of about 400 Tbit/s for 400 Gbit/s requests and a 1% BP obtained in [16].

The transport capacity obtained for the three modulation formats and the three MB architectures, for the target BP of 1%, is shown in Figs. 12 and 13, respectively, for the BT-UK and CONUS-60 networks. To maximize the transport capacity, the channel launch power considered for the baseline architecture is −2 dBm, and for the common-band and compact architectures is 0 dBm, considering the BT-UK network. In the case of the CONUS-60 network, the channel launch power is 0 dBm for all MB architectures. Table 6 shows the number of allocated demands for each modulation format, MB architecture, and network topology.

From Fig. 12, it can be observed that for the baseline architecture, the transport capacity for the three modulation formats is not as balanced as the one obtained for the common-band and compact architectures, with the QPSK format being the dominant modulation format. For the common-band and compact architectures, there is a higher balance between the transport capacity of the three modulation formats because the channel launch power (0 dBm) is higher than in the baseline architecture (−2 dBm) and with more power, higher modulation formats can be used.

Fig. 13 shows that, for all MB node architectures, the QPSK transport capacity is higher compared to the remaining modulation formats due to the average longer link length of the CONUS-60 network. Also, the 16-QAM transport capacity is higher than the 8-QAM transport capacity due to a similar number of allocated demands obtained for both modulations (see Table 6). From Figs. 12 and 13, it is possible to see that the QPSK transport capacity is more preponderant in the CONUS-60 network than in the BT-UK network, due to the difference of network sizes. For the BT-UK network, a network with shorter link lengths and more meshed, a more balanced assignment of the modulation formats is observed.

4.4. Total network cost-per-bit

In this subsection, we compute and discuss the total network cost-per-bit for the MB architectures analyzed in the previous subsection, considering the BT-UK and the CONUS-60 networks. The total network cost-per-bit is computed using Eq. (10) and is normalized to the cost-per-bit obtained with the baseline architecture, for a zero fiber lease cost, a launch power of −2 dBm, and a target BP of 1%. The reference

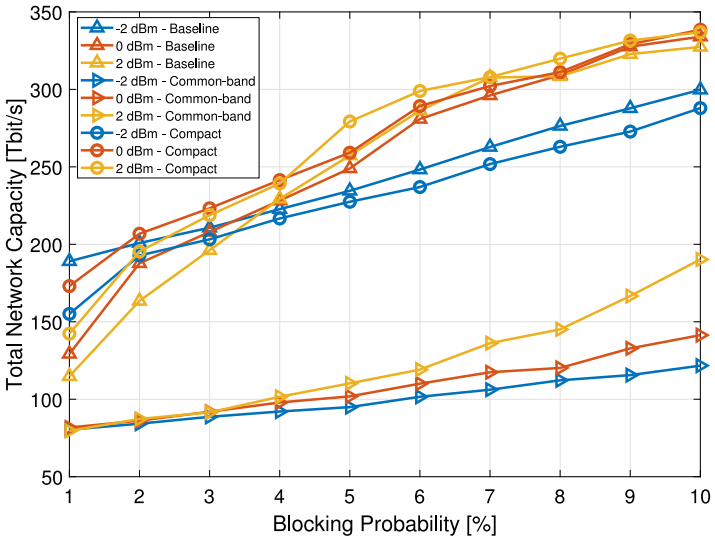

Fig. 10. Total network capacity as a function of the BP, for the BT-UK network considering the baseline, common-band and compact MB node architectures, and the channel launch powers of −2, 0, and 2 dBm.

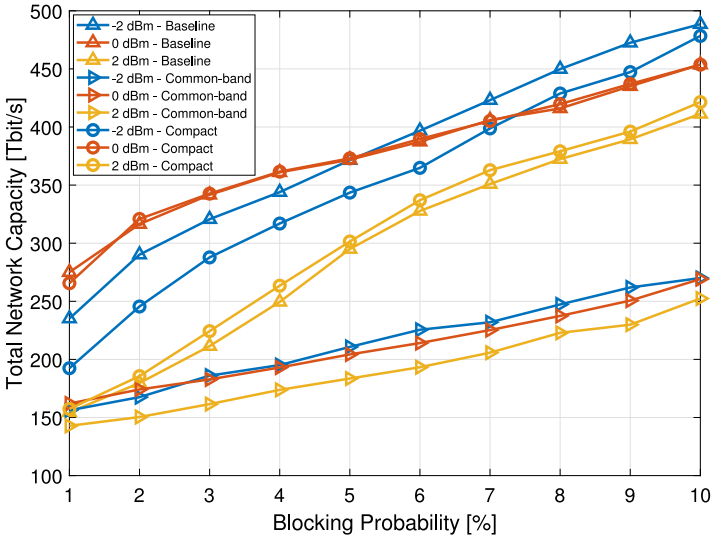

Fig. 11. Total network capacity as a function of the BP, for the CONUS-60 network considering the baseline, common-band and compact MB node architectures, and the channel launch powers of −2, 0, and 2 dBm.

Table 6
Number of allocated demands for each modulation format and MB architecture, for a BP of 1%.

Architecture	Number of allocated demands per modulation format					
	BT-UK			CONUS-60		
	QPSK	8-QAM	16-QAM	QPSK	8-QAM	16-QAM
Baseline	424	167.5	133.5	841.5	147.5	152
Common-band	116	77	87	500	90	89
Compact	303	204	151.5	814.5	150	148.5

cost-per-bit of the BT-UK network is obtained considering a total network cost of 157461 and a total network capacity of 189.06 Tbit/s for the BP of 1% and the baseline architecture (see Fig. 10). The reference cost-per-bit of the CONUS-60 network is obtained for a total network cost of 349260 and a total network capacity of 235.142 Tbit/s (see Fig. 11).

Fig. 14 shows the normalized cost-per-bit as a function of the fiber lease cost for the three MB architectures, channel launch powers of −2, 0, and 2 dBm, and the target BP of 1%, considering the BT-UK topology. From Fig. 14, it can be observed that, for all channel powers, the common-band architecture has the highest total cost-per-bit (above 2) due to the lower total network capacity achieved, compared with the normalized cost-per-bit of the baseline and compact architectures. For the common-band architecture, all channel launch powers lead to a similar cost-per-bit. For the baseline and compact architectures, the most cost-per-bit effective channel launch powers are, respectively, −2 and 0 dBm. For the real fiber lease cost of 0.33 [13], the baseline architecture leads to the lowest cost-per-bit of 1.1, for the −2 dBm channel launch power.

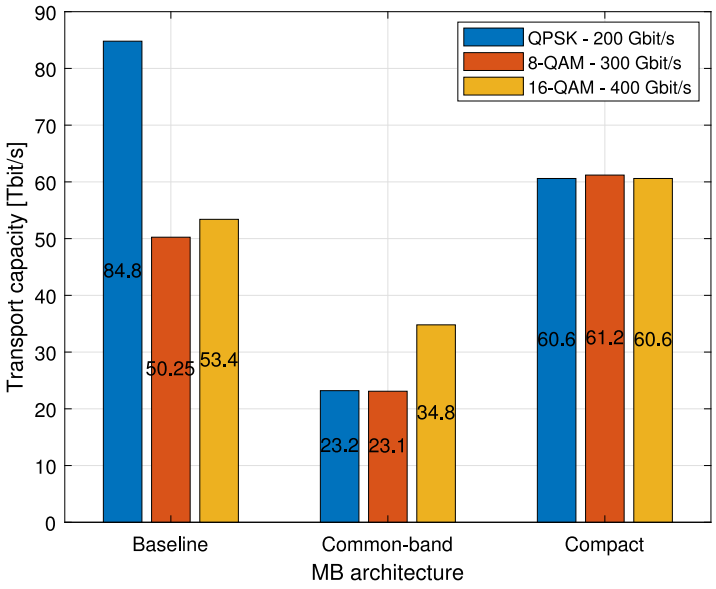

Fig. 12. Transport capacity distribution among the 3 modulation formats considered for the baseline (−2 dBm), common-band (0 dBm), and compact (0 dBm) architectures, considering the BT-UK network and a 1% BP.

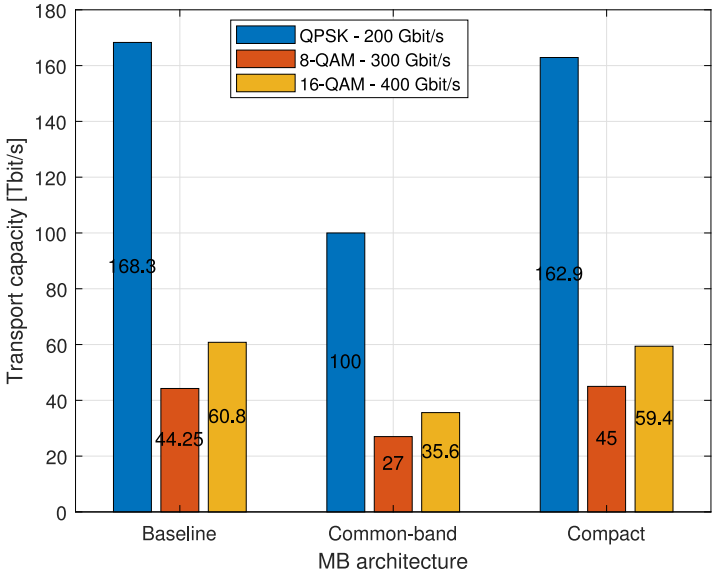

Fig. 13. Transport capacity distribution among the 3 modulation formats considered for the baseline (0 dBm), common-band (0 dBm), and compact (0 dBm) architectures, considering the CONUS-60 network and a 1% BP.

Fig. 15 shows the normalized cost-per-bit of the CONUS-60 network, for the three MB architectures, channel launch powers of −2, 0, and 2 dBm, and the target BP of 1%. From Fig. 15, it can be seen that the channel launch power of 0 dBm leads to the lower cost-per-bit for the three MB architectures. For this power, the baseline and compact architectures have a much lower cost-per-bit (about 0.6 less expensive) than the common-band architecture. For the real fiber lease cost of 0.33 [13], the baseline architecture for a channel launch power of 0 dBm leads to the lowest network cost-per-bit (1.14) in comparison with the other two architectures.

Comparing the total network cost-per-bit of Figs. 14 and 15, it can be seen that the total network cost-per-bit for all MB architectures in the CONUS-60 network has a sharper increase with the fiber lease cost than for the BT-UK network, since the CONUS-60 network has a higher number of nodes and longer average link length. The most cost-per-bit effective channel launch power of the baseline architecture for the BT-UK network (−2 dBm) is lower than the one obtained for the CONUS-60 (0 dBm), since the CONUS-60 network demands a higher channel launch power to achieve a lower total cost-per-bit. In the case of common-band and compact architectures, the same cost-per-bit effective channel launch power (0 dBm) is obtained, for both network topologies.

The total network cost-per-bit obtained in Figs. 14 and 15 for the best scenario (lower cost-per-bit obtained for a specific channel launch power) reveals that the total network cost-per-bit including the PLIs impact, obtained for the common-band architecture is higher than the total network cost-per-bit obtained for the remaining MB architectures. Without the influence of the PLIs, as shown in Fig. 2, the common-band architecture has the lowest cost-per-bit. So, it can be concluded that in a network scenario, when the PLIs are considered, this cost advantage vanishes. Regarding the baseline and compact architectures, the total cost-per-bit obtained in Fig. 2, for both architectures is very similar. However, in a network scenario, considering the PLIs impact, the total

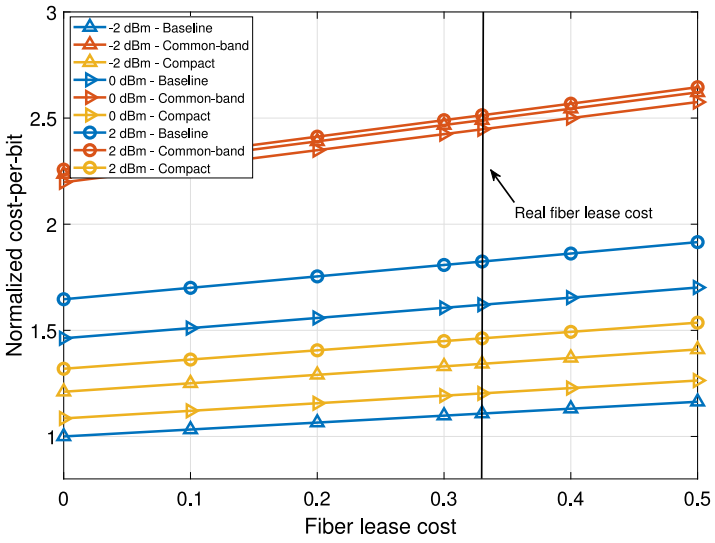

Fig. 14. Normalized cost-per-bit as a function of the fiber lease cost considering the BT-UK network and a BP of 1%, for the baseline, common-band and compact architectures.

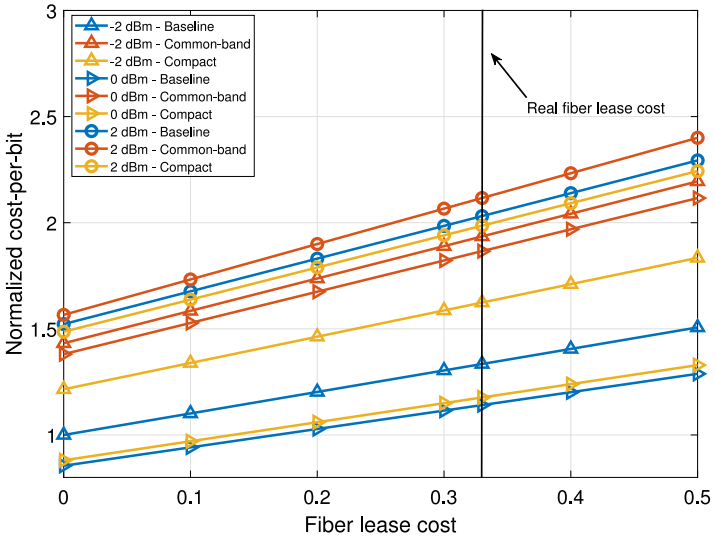

Fig. 15. Normalized cost-per-bit as a function of the fiber lease cost considering the CONUS-60 network and a BP of 1%, for the baseline, common-band and compact architectures.

cost-per-bit of the baseline architecture becomes slightly lower than the compact architecture cost-per-bit.

Finally, comparing the results obtained in Figs. 14 and 15 with Figure 3 of [11], for α=1.5, β=2, it can be observed that the total network cost-per-bit obtained in this work, follows the same behavior with the fiber lease cost as the one presented in [11]. For the best channel launch powers of −2 dBm (baseline architecture) and 0 dBm (common-band architecture), and the BT-UK topology (similar to the NSFNET topology, in terms of the number of nodes and average node degree [11]), the total network cost-per-bit obtained in this work, for the common-band architecture is approximately twice the baseline architecture cost-per-bit, while, in [11], the common-band architecture has a lower cost-per-bit (0.8 times below the baseline cost-per-bit). This worst performance of the common-band architecture observed in our work is due to the impact of the additional ASE noise coming from the amplifiers inside the AO-WC, which degrades significantly the OSNR, lowers the total network capacity, and increases the cost-per-bit. As this behavior is not seen in [11], we suspect that this additional noise has not been taken into account in [11].

5. Conclusions

In this work, we first studied and compared several C+L+S MB node architectures in terms of their internal structure, cost-per-bit, and insertion losses. Next, two network scenarios, the BT-UK and CONUS-60, were studied with the baseline, common-band, and compact node architectures. To accomplish this study, we have developed a network planning tool that solves the RMSA problem, taking into account the PLIs and the MB node architecture impact. The total network capacity, as well as the total network cost-per-bit, have been assessed for several BPs.

We have concluded that the AO-WC node architecture presents the highest cost-per-bit due to the high number of AO-WCs. The common-band architecture presents a slightly lower cost-per-bit compared with the baseline and compact MB node architectures. Nevertheless, in a network scenario where the PLIs are included, it is shown in this work that the common-band node architecture is the most expensive. The common-band architecture has the lowest total network capacity as it is hugely impacted by the PLIs, in particular by the additional ASE noise from the AO-WCs. For a BP of 1% and the channel launch power

that guarantees the highest total network capacity, the common-band total network capacity is at least 91 Tbit/s lower than the baseline and compact total network capacities for both network topologies. Both compact and baseline MB node architectures have similar total network capacity and costs, with and without the PLIs.

For an immediate network deployment, the MB baseline architecture seems advantageous over the compact architecture due to its mature technology and slightly lower cost-per-bit. Nevertheless, the compact architecture could be important in the future, as it has the switching capability between bands and requires a much lower number of components. Both the AO-WC and common-band architectures critically depend on the AO-WC, which is not in a commercial phase and has high insertion losses and costs.

CRediT authorship contribution statement

João Frederico Ó Ramos: Formal analysis, Data curation, Investigation, Software, Validation, Visualization, Writing – original draft, Writing – review & editing. **Luís Cancela:** Conceptualization, Data curation, Formal analysis, Investigation, Methodology, Project administration, Resources, Supervision, Validation, Visualization, Writing – review & editing. **João Rebola:** Methodology, Investigation, Formal analysis, Data curation, Conceptualization, Validation, Visualization, Writing – review & editing, Project administration, Resources, Supervision.

Declaration of competing interest

The authors declare that they have no known competing financial interests or personal relationships that could have appeared to influence the work reported in this paper.

Data availability

No data was used for the research described in the article.

Acknowledgment

This research received no external funding.

Appendix A. Supplementary data

Supplementary material related to this article can be found online at https://doi.org/10.1016/j.yofte.2024.103815.

References

[1] P.J. Winzer, D.T. Neilson, From scaling disparities to integrated parallelism: a decathlon for a decade, J. Lightwave Technol. 35 (5) (2017) 1099–1115.
[2] N. Deng, L. Zong, H. Jiang, Y. Duan, K. Zhang, Challenges and enabling technologies for multi-band WDM optical networks, J. Lightwave Technol. 40 (11) (2022) 3385–3394.
[3] T. Hoshida, V. Curri, L. Galdino, D.T. Neilson, W. Forysiak, J.K. Fischer, T. Kato, P. Poggiolini, Ultrawideband systems and networks: beyond C+L-band, Proc. IEEE 110 (11) (2022) 1725–1741.
[4] W. Klaus, P.J. Winzer, K. Nakajima, The role of parallelism in the evolution of optical fiber communication systems, Proc. IEEE 110 (11) (2022) 1619–1654.
[5] B. Correia, R. Sadeghi, E. Virgillito, A. Napoli, N. Costa, J. Pedro, V. Curri, Power control strategies and network performance assessment for C+L+S multiband optical transport, J. Opt. Commun. Netw. 13 (7) (2021) 147–157.
[6] D.T. Hai, On routing, wavelength, network coding assignment, and protection configuration problem in optical-processing-enabled networks, IEEE Trans. Netw. Serv. Manag. 20 (3) (2023) 2504–2514.
[7] A.E. Willner, A. Fallahpour, F. Alishahi, Y. Cao, A. Mohajerin-Ariaei, A. Almaiman, P. Liao, K. Zou, A.N. Willner, M. Tur, All-optical signal processing techniques for flexible networks, J. Lightwave Technol. 37 (1) (2019) 21–35.
[8] M. Cantono, R. Schmogrow, M. Newland, V. Vusirikala, T. Hofmeister, Opportunities and challenges of C+L transmission systems, J. Lightwave Technol. 38 (5) (2020) 1050–1060.
[9] H. Kawahara, M. Nakagawa, T. Seki, T. Miyamura, Experimental demonstration of wavelength-selective band/direction-switchable multi-band OXC using an inter-band all-optical wavelength converter, in: European Conference on Optical Communications, ECOC, Brussels, Belgium, 2020, http://dx.doi.org/10.1109/ECOC48923.2020.9333270.
[10] M. Nakagawa, H. Kawahara, T. Seki, T. Miyamura, Adaptive link-by-link band allocation: a novel adaptation scheme in multi-band optical networks, in: International Conference on Optical Network Design and Modeling, ONDM, Gothenburg, Sweden, 2021, http://dx.doi.org/10.23919/ONDM51796.2021.9492502.
[11] M. Nakagawa, T. Seki, T. Miyamura, Techno-economic potential of wavelength-selective band-switchable OXC in S+C+L band optical ntworks, in: Optical Fiber Communications Conference and Exhibition, OFC, San Diego, CA, USA, 2022, http://dx.doi.org/10.1364/OFC.2022.W2A.24.
[12] S. Yamamoto, H. Taniguchi, Y. Kisaka, S. Camatel, Y. Ma, D. Ogawa, K. Hadama, M. Fukutoku, T. Goh, K. Suzuki, First demonstration of a C+L band CDC-ROADM with a simple node configuration using multiband switching devices, Opt. Express 29 (22) (2021) 36353–36365.
[13] R.K. Jana, A. Mitra, A. Pradhan, K. Grattan, A. Srivastava, B. Mukherjee, A. Lord, When is operation over C+L bands more economical than multifiber for capacity upgrade of an optical backbone network? in: European Conference on Optical Communications, ECOC, Brussels, Belgium, 2020, http://dx.doi.org/10.1109/ECOC48923.2020.9333276.
[14] J.M. Simmons, Optical Network Design and Planning, second ed., Springer International Publishing, 2014, http://dx.doi.org/10.1007/978-3-319-05227-4.
[15] A. Souza, N. Costa, J. Pedro, J. Pires, Comparison of fast quality of transmission estimation methods for C+L+S optical systems, J. Opt. Commun. Netw. 15 (11) (2023) 1–12.
[16] R. Sadeghi, B. Correia, A. Souza, N. Costa, J. Pedro, A. Napoli, V. Curri, Transparent vs translucent multi-band optical networking: capacity and energy analyses, J. Lightwave Technol. 40 (11) (2022) 3486–3498.
[17] J.F. Ramos, L. Cancela, J. Rebola, Influence of the ROADM architecture on the cost-per-bit in C+L+S multi-band optical networks, in: 2023 23rd International Conference on Transparent Optical Networks, ICTON, 2023, http://dx.doi.org/10.1109/ICTON59386.2023.10207552.
[18] Y. Ma, L. Stewart, J. Armstrong, I.G. Clarke, G. Baxter, Recent progress of wavelength selective switch, J. Lightwave Technol. 39 (4) (2021) 896–903.
[19] N.K. Fontaine, M. Mazur, R. Ryf, H. Chen, L. Dallachiesa, D.T. Neilson, 36-THz bandwidth wavelength selective switch, in: 2021 European Conference on Optical Communication, ECOC, 2021, http://dx.doi.org/10.1109/ECOC52684.2021.9606114.
[20] T. Kato, et al., Multi-band WDM transmission technology exceeding transceiver wavelength band, in: 2020 Opto-Electronics and Communications Conference, OECC, 2020, http://dx.doi.org/10.1109/OECC48412.2020.9273578.
[21] T. Yamauchi, T. Kato, G. Nakagawa, S. Watanabe, Y. Akiyama, T. Hoshida, Investigation on maximum transmission reach in wavelength converted systems, in: 2019 24th OptoElectronics and Communications Conference (OECC) and 2019 International Conference on Photonics in Switching and Computing, PSC, 2019, http://dx.doi.org/10.23919/PS.2019.8818124.
[22] T. Kato, S. Watanabe, T. Yamauchi, G. Nakagawa, H. Muranaka, Y. Tanaka, Y. Akiyama, T. Hoshida, Real-time transmission of 240×200-Gb/s signal in S+C+L triple-band WDM without S- or L-band transceivers, in: 45th European Conference on Optical Communication, ECOC 2019, 2019, http://dx.doi.org/10.1049/cp.2019.1021.
[23] Series A Family of Programmable Optical Processors, Finisar Corporation, II-IV, WaveShaper, 2020.
[24] V. Curri, M. Cantono, R. Gaudino, Elastic all-optical networks: a new paradigm enabled by the physical layer. How to optimize network performances? J. Lightwave Technol. 35 (6) (2017) 1211–1221.
[25] E. Amir, K-shortest paths in a graph represented by a sparse matrix (Yen's algorithm), 2013, URL: https://www.mathworks.com/matlabcentral/fileexchange/35397-k-shortest-paths-in-a-graph-represented-by-a-sparse-matrix-yen-s-algorithm.
[26] J. Pedro, S. Pato, Capacity increase and hardware savings in DWDM networks exploiting next-generation optical line interfaces, in: 2018 20th International Conference on Transparent Optical Networks, ICTON, 2018, http://dx.doi.org/10.1109/ICTON.2018.8473705.
[27] J. Pedro, Designing transparent flexible-grid optical networks for maximum spectral efficiency, J. Opt. Commun. Netw. 9 (4) (2017) 35–44.
[28] T. Rahman, A. Napoli, D. Rafique, B. Spinnler, M. Kuschnerov, I. Lobato, B. Clouet, M. Bohn, C. Okonkwo, H. de Waardt, On the mitigation of optical filtering penalties originating from ROADM cascade, IEEE Photonics Technol. Lett. 26 (2) (2014) 154–157.
[29] D. Semrau, R.I. Killey, P. Bayvel, A closed-form approximation of the Gaussian noise model in the presence of inter-channel stimulated raman scattering, J. Lightwave Technol. 37 (9) (2019) 1924–1936.

[30] D. Semrau, E. Sillekens, R.I. Killey, P. Bayvel, A modulation format correction formula for the Gaussian noise model in the presence of inter-channel stimulated raman scattering, J. Lightwave Technol. 37 (19) (2019) 5122–5131.

[31] D. Semrau, E. Sillekens, R.I. Killey, P. Bayvel, Corrections to "A modulation format correction formula for the Gaussian noise model in the presence of inter-channel stimulated raman scattering", J. Lightwave Technol. 38 (6) (2020) 1604.

[32] OpenZR+ specifications, v. 3.0 (2023), 2023, URL: https://openzrplus.org/documents/.